Isotope Effects in the Reactions of Chloroform Isotopologues with Cl, OH, and OD

ARTICLE *in* THE JOURNAL OF PHYSICAL CHEMISTRY A · MARCH 2009

Impact Factor: 2.69 · DOI: 10.1021/jp807233x · Source: PubMed

3 AUTHORS, INCLUDING:

Elna Nilsson
Lund University
47 PUBLICATIONS **340** CITATIONS
SEE PROFILE

Matthew S Johnson
University of Copenhagen
138 PUBLICATIONS **1,683** CITATIONS
SEE PROFILE

Article

Isotope Effects in the Reactions of Chloroform Isotopologues with Cl, OH, and OD

Elna J. K. Nilsson, Matthew S. Johnson, and Claus J. Nielsen

J. Phys. Chem. A, **2009**, 113 (9), 1731-1739• DOI: 10.1021/jp807233x • Publication Date (Web): 10 February 2009

Isotope Effects in the Reactions of Chloroform Isotopologues with Cl, OH, and OD

Elna J. K. Nilsson,*,† Matthew S. Johnson,† and Claus J. Nielsen‡

Copenhagen Center for Atmospheric Research, Department of Chemistry, University of Copenhagen, Universitetsparken 5, 2100 Copenhagen, Denmark, and Centre for Theoretical and Computational Chemistry, Department of Chemistry, University of Oslo, P.O. Box 1033 Blindern, 0315 Oslo, Norway

Received: August 13, 2008; Revised Manuscript Received: January 5, 2009

The kinetic isotope effects in the reactions of $CHCl_3$, $CDCl_3$, and $^{13}CHCl_3$ with Cl, OH, and OD radicals have been determined in relative rate experiments at 298 ± 1 K and atmospheric pressure monitored by long path FTIR spectroscopy. The spectra were analyzed using a nonlinear least-squares spectral fitting procedure including line data from the HITRAN database and measured infrared spectra as references. The following relative reaction rates were determined: $k_{CHCl_3+Cl}/k_{CDCl_3+Cl} = 3.28 \pm 0.01$, $k_{CHCl_3+Cl}/k_{^{13}CHCl_3+Cl} = 1.000 \pm 0.003$, $k_{CHCl_3+OH}/k_{CDCl_3+OH} = 3.73 \pm 0.02$, $k_{CHCl_3+OH}/k_{^{13}CHCl_3+OH} = 1.023 \pm 0.002$, $k_{CHCl_3+OD}/k_{CDCl_3+OD} = 3.95 \pm 0.03$, and $k_{CHCl_3+OD}/k_{^{13}CHCl_3+OD} = 1.032 \pm 0.004$. Larger isotope effects in the OH reactions than in the Cl reactions are opposite to the trends for CH_4 and CH_3Cl reported in the literature. The origin of these differences was investigated using electronic structure calculations performed at the MP2/aug-cc-PVXZ (X = D, T, Q) level of theory and are compared with previously calculated values for the other methane derivatives. The Born−Oppenheimer barrier heights to H abstraction are 12.2 and 17.0 kJ mol^{-1} at the CCSD(T)/aug-cc-pVTZ level of theory for OH and Cl, respectively. The reaction rate coefficients of the two elementary vapor phase reactions including the ^2H and ^{13}C kinetic isotope effects were calculated using improved canonical variational theory with small curvature tunneling (ICVT/SCT) and the results compared with experimental data.

1. Introduction

The average global atmospheric concentration of chloroform has, on the basis of data from nine years of field measurements, been calculated to be 18.5 pptv with seasonal, altitudinal, and latitudinal variability.[1] This variability is the result of short lifetime of ca. 6 months for chloroform in the atmosphere because of its reaction with hydroxyl radicals.[2] Global atmospheric chloroform budgets have been presented by several groups.[1−3] The inventories of McCulloch and of Khalil and Rasmussen agree in setting the total emission of chloroform to be 660 ± 220 Gg yr^{-1} and 350−600 Gg yr^{-1}, respectively.

Anthropogenic sources of chloroform are mainly from the pulp and paper industry and from drinking and wastewater treatment, with a smaller contribution from the pharmaceutical industry.[1,2,4] Some discrepancies can be found in the literature concerning the magnitude of the anthropogenic contribution. A value of 10% of the total is reported by several groups.[1,2,4] A recent study reports that around 1990, 50% of atmospheric chloroform had an anthropogenic origin and that this has declined to about 29% more recently.[3] According to Worton et al.,[3] the error in the numbers reported earlier is due to an overestimation of the natural sources of chloroform to the atmosphere. A decrease in atmospheric chloroform since about 1990 is also reported by Trudinger et al.[5]

The dominant natural source is an unidentified, probably biological, process in the oceans, whereas soil processes constitute the second most important contribution.[2,6] McCulloch reports yearly contributions of chloroform from oceans and soil processes to be 360 ± 90 Gg and 220 ± 100 Gg, respectively. Other sources, such as geological contributions and anaerobic fermentation contribute only a few gigagrams per year.[2] In summary, the uncertainties in the natural sources are large.

The main atmospheric sink for chloroform is reaction with hydroxyl radicals; other processes such as aerobic degradation and dechlorination by methanogens in soil and sediment are not significant loss processes on the global scale but may have local importance.[2,7] Small amounts of chloroform are transported to the stratosphere, where photolysis is the most important removal process.[1] The reaction of chloroform with hydroxyl radicals is estimated to be the largest source of phosgene, CCl_2O, to the atmosphere.[8]

Whereas chloroform is not classified as a greenhouse gas or considered to be a threat to the ozone layer, its reactivity is important for understanding the behavior of the chlorinated methane derivatives. The other methane derivatives, methyl chloride, CH_3Cl, methylene chloride, CH_2Cl_2, and carbon tetrachloride, CCl_4, all have important environmental effects.

A number of absolute and relative rate studies have been reported for the $CHCl_3$ + Cl and $CHCl_3$ + OH reactions. The Cl reaction has been studied at room temperature[8,9] and over temperature ranges of 222−298[10] and 297−854 K.[11] The OH reaction has been studied at room temperature[12] and in the temperature ranges 245−375,[13] 295−955,[14] and 293−358 K.[15] The currently recommended rate constants at 298 K are (1.20 ± 0.18) × 10^{-13} for the Cl reaction and (1.00 ± 0.15) × 10^{-13} cm^3 $molecule^{-1}$ s^{-1} for the OH reaction.[16]

In a theoretical investigation of the interaction of OH with chloroform at the MP2/6-31+G(d,p) level of theory, the barrier height of the reaction could not be determined, which the authors interpret as being a consequence of its flatness.[17,18] A recent report on the effect of isotopic substitution on vibrational

* Corresponding author. E-mail: elna@kiku.dk.
† University of Copenhagen.
‡ University of Oslo.

10.1021/jp807233x CCC: $40.75
Published on Web 02/10/2009

TABLE 1: Components Included in Spectral Fit for the Different Reaction Mixtures and Wavelength Ranges Used in the Analyses

reaction mixture	wavelength range (cm^{-1})	components
$CHCl_3/CDCl_3/Cl$	710−1260	$CHCl_3$, $CDCl_3$, CCl_2O
$CHCl_3/^{13}CHCl_3/Cl$	710−1260	$CHCl_3$, $^{13}CHCl_3$, CCl_2O, $^{13}CCl_2O$
$CHCl_3/CDCl_3/OH$	710−950	$CHCl_3$, $CDCl_3$, O_3, CO_2, CCl_2O
$CHCl_3/^{13}CHCl_3/OH$	710−800	$CHCl_3$, $^{13}CHCl_3$, O_3, CO_2, CCl_2O, $^{13}CCl_2O$
$CHCl_3/CDCl_3/OD$	710−950	$CHCl_3$, $CDCl_3$, O_3, CO_2, CCl_2O
$CHCl_3/^{13}CHCl_3/OD$	710−795	$CHCl_3$, $^{13}CHCl_3$, O_3, CCl_2O, $^{13}CCl_2O$

frequencies of chloroform and chloromethane is in good agreement with experimental values.[19]

The large uncertainties in the atmospheric budget of chloroform indicate the need for a better understanding of the sources and sinks. Knowledge about the stable isotope composition of chloroform, and fractionation factors in atmospherically relevant reactions can be used as a tool in the determination of the atmospheric chloroform budget.[20] In the present work, we report determinations of kinetic isotope effects in the reactions of chloroform with the atmospherically important radicals Cl and OH. The OD radical has also been investigated to give additional information on the reaction.

2. Experimental and Computational Methods

2.1. Relative Rate Experiments. The relative rate method can be used if there are no other reactions other than the investigated one that consume the reactants to a significant degree. If this is true, then the following expression is valid

$$\ln\left(\frac{[A]_0}{[A]_t}\right) = \frac{k_A}{k_B}\ln\left(\frac{[B]_0}{[B]_t}\right) \quad (1)$$

where $[A]_0$, $[A]_t$, $[B]_0$, and $[B]_t$ are the concentrations of the compounds at times 0 and t. In a plot of $\ln([A]_0/[A]_t)$ versus $\ln([B]_0/[B]_t)$, the slope will equal the relative rate of the reaction.

Relative rate experiments were carried out in a 250 L electropolished stainless steel smog chamber equipped with a White-type multipass mirror system giving an optical path length of 120 m. UV lamps were mounted in a quartz tube in the reaction chamber. The components of the reaction mixtures were introduced to the chamber via a Pyrex gas handling system by flushing with synthetic air (AGA 4.0). Chloroform isotopologue concentrations were in the range of 1.3 to 3.0 ppm and standard laboratory grade Cl_2 was in the range of 2.0 to 10.0 ppm. Chloroform and Cl_2 gas were purified by several freeze−pump−thaw cycles before being introduced to the reaction chamber. Volume fractions of H_2 (AGA 4.5) and ozone in the OH experiments were around 3×10^3 and 400 ppm, respectively. Additional synthetic air was flushed into the reaction chamber until a final pressure of about 1013 mbar was reached.

The consumption of reactants was monitored using Fourier transform infrared spectroscopy (FTIR). The spectra were recorded using a Bruker IFS 66v infrared spectrometer with a liquid-nitrogen-cooled MCT detector at a resolution of 0.5 cm^{-1}. For each spectrum, 128 scans were coadded to give an acceptable signal-to-noise ratio, and the interferograms were Fourier transformed using boxcar apodization. During each experiment, the reaction mixture was photolyzed 7−15 times, giving a total photolysis time of 2 to 3 h. Each photolysis step was followed by a stabilization time, typically two minutes, before the FTIR spectrum was recorded. The experiments were terminated when around 50% of the reactant species were consumed. For each reaction, the experiment was repeated three to four times. To check for possible dark reactions, the reaction mixture was left in the cell during a time period corresponding to a standard experiment; no change in the composition of the reaction mixture was detected during this time period. Photolysis experiments with only chloroform in the cell show that the compound is not photolyzed by the lamps used to initiate the radical species. This is consistent with the published UV-absorption cross section of chloroform.[16]

2.2. Chemicals and Radical Production. The chloroform isotopomers used in the study, $CHCl_3$, $CDCl_3$ (99.8 atom % D, Aldrich), and $^{13}CHCl_3$ (99 atom % ^{13}C, Isotech), where purified by three freeze−pump−thaw cycles. $CHCl_3$ was stabilized by 1% ethanol; this was removed by the addition of a small amount of concentrated sulfuric acid.

OH radicals were produced by photolysis of a mixture of O_3 and H_2 (AGA 4.0)

$$O_3 + h\nu \rightarrow O(^1D) + O_2 \quad (2)$$

$$O(^1D) + H_2 \rightarrow OH + H \quad (3)$$

$$H + O_3 \rightarrow OH + O_2 \quad (4)$$

$$H + O_2 \rightarrow HO_2 \quad (5)$$

$$HO_2 + O_3 \rightarrow OH + 2O_2 \quad (6)$$

Ozone was produced from O_2 (AGA 5.0) using a MK II ozone generator from BOC. The photolysis was carried out using a Philips TUV 30 W lamp with $\lambda_{max} \approx 254$ nm. Reaction 3 lead to the production of OH radicals in both the ground and excited vibrational states.[21−23] Literature values for the collisional quenching rates of vibrationally excited OH by O_2 and N_2 are 10^{-15} and 10^{-13} cm^3 $molecule^{-1}$ s, respectively,[24] which is comparable to the OH reaction rate with $CHCl_3$. However, the concentrations of O_2 and N_2 are 10^5 times higher than that of $CHCl_3$. It can therefore be concluded that $CHCl_3$ almost exclusively reacts with OH in the vibrational ground state.

OD radicals were produced by the same procedure using D_2 (99.8 atom % D, Isotech).

Cl atoms were produced by the photolysis of Cl_2 using two Philips TLD-08 fluorescence lamps, $\lambda_{max} \approx 350$ nm, and leading to the production of ground-state chlorine atoms

$$Cl_2 + h\nu \rightarrow 2Cl \quad (7)$$

2.3. Data Analysis and Reference Spectra. The spectra for the different reaction mixtures were analyzed using a nonlinear least-squares spectral fitting procedure developed by D. Griffith.[25] The spectral regions analyzed (C−H bending and C−Cl stretching regions) and the components used in the analysis are given in Table 1. H_2O and HOCl spectra for the analysis were taken from the HITRAN database,[26] whereas for the other components, high-resolution FTIR spectra were used. These reference spectra were produced using the same equipment as that used in the relative rate experiments but with a resolution of 0.25 cm^{-1} and 512 scans. The sample of $^{13}CCl_2O$ was produced in situ by complete conversion of $^{13}CHCl_3$.

2.4. Electronic Structure Calculations. Electronic structures and vibrational frequencies for reactants, first-order saddle

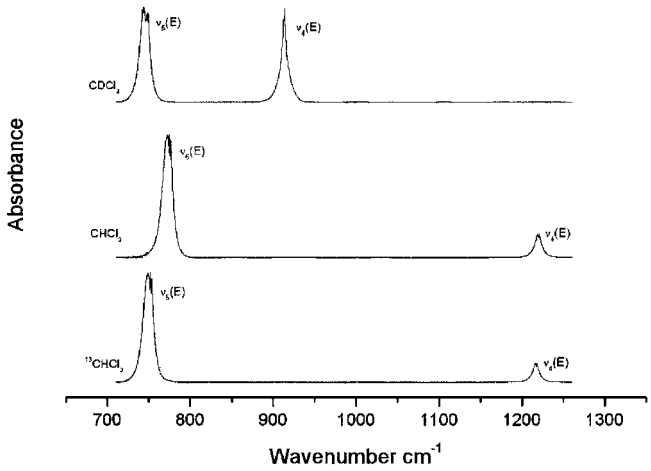

Figure 1. FTIR spectra in the C−H region of $CDCl_3$, $CHCl_3$, and $^{13}CHCl_3$ showing the ν_4 and ν_5 bands.

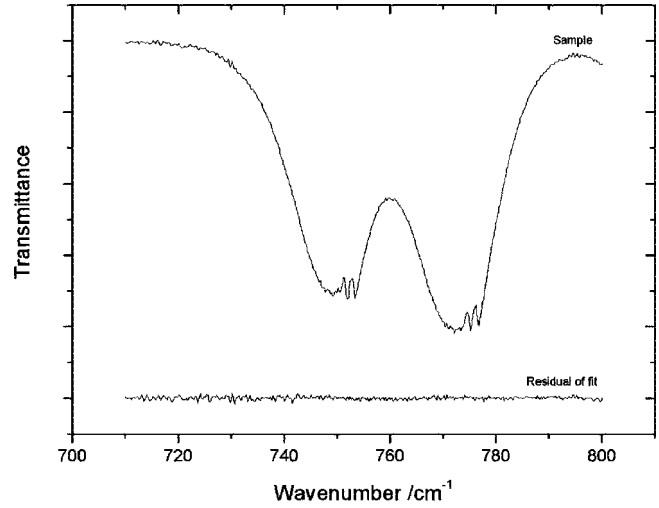

Figure 2. FTIR spectra of a mixture of $CHCl_3$ and $^{13}CHCl_3$ during reaction with Cl.

points, and products in the reactions of chloroform with chlorine and hydroxyl radicals were calculated at the MP2 and CCSD(T) levels of theory using Dunning's correlation consistent aug-cc-PVXZ (X = D, T), basis sets. The Gaussian 03 software package was used for the calculations.[27]

The saddle points of the reactions were found using the QSTN method. The minimum energy path connecting the transition states to reactants and products was computed using the intrinsic reaction coordinate (IRC) method[28] with a step size of 0.02 $u^{1/2}$ Bohr. QST and IRC calculations were performed using the aug-cc-PVDZ basis set. Hessians were calculated at nonstationary points along the reaction paths at the same level of theory.

2.5. Calculations of Rate Coefficients. The rate coefficients were calculated using interpolated variational transition-state theory by mapping (IVTST-M)[29] using data from the electronic structure and frequency calculations.

Rate coefficients were calculated in the range of 200−1000 K using the POLYRATE program.[30] The rates for the isotopically substituted reactions were calculated according to the method of Fast et al.[31] In addition to conventional transition state theory (TST), calculations were also performed using canonical variational transition state theory (CVT) and canonical unified statistical theory (CUS).[32] The small curvature tunneling approach (SCT) was used to represent the tunneling effect. Energies for nonstationary points along the minimum energy path calculated at the MP2/aug-cc-PVDZ level were corrected using the ISPE[33] method, with CCSD(T)/aug-cc-PVTZ energies computed at stationary points. Frequencies at the MP2/aug-cc-PVDZ level were scaled using a factor of 0.959.

For the chlorine atom, two electronic states, separated by 882 cm^{-1} and with degeneracies of four and two, were included in the calculation of its electronic partition function. The OH radical has two electronic states separated by 140 cm^{-1}, both with a degeneracy of two, that were included in the calculations.

The C−H−OH torsional mode in the transition state of the $CHCl_3$ + OH reaction was treated anharmonically using the hindered rotor method.[34]

3. Results and Discussion

3.1. Experimental Study. Figure 1 shows the FTIR spectra of the three chloroform isotopologues in the C−H bending region. The ν_5(E) band of $CHCl_3$, situated around 775 cm^{-1}, overlaps with the corresponding bands for both $CDCl_3$ (747 cm^{-1}) and $^{13}CHCl_3$ (752 cm^{-1}), but the peaks are separated enough that analysis is straightforward. The ν_4(E) band of $CDCl_3$, located around 915 cm^{-1}, is well separated from the corresponding band for $CHCl_3$, at about 1220 cm^{-1}. The ν_4(E) band of $^{13}CHCl_3$ (1217 cm^{-1}) overlaps with the corresponding band for $CHCl_3$, but the bands are sufficiently separated to make an analysis possible.

Relative rate data for the investigated reactions are presented in the following sections. The relative rate plots contain data from three or four independent experiments.

3.1.1. Cl Radical Reaction. The stable products of the reaction between chloroform and Cl radicals are hydrochloric acid, HCl, and phosgene, CCl_2O. Reactions 8 to 11 below show the steps in the reaction mechanism resulting in the phosgene product.

$$CHCl_3 + Cl \rightarrow CCl_3 + HCl \quad (8)$$

$$CCl_3 + O_2 \rightarrow OOCCl_3 \quad (9)$$

$$OOCCl_3 + OOCCl_3 \rightarrow 2OCCl_3 + O_2 \quad (10)$$

$$OCCl_3 \rightarrow CCl_2O + Cl \quad (11)$$

None of the products complicate the analysis of IR spectra. The HCl bands fall outside the spectral range used for analysis. Phosgene has its strong $\nu_4(B_1)$ band around 850 cm^{-1}, and there is essentially no overlap with the chloroform isotopologues. Figure 2 shows an example of an FTIR spectrum of the analyzed region of a mixture of $CHCl_3$ and $^{13}CHCl_3$ during reaction.

Relative rate plots of the decay of mixtures of $CHCl_3$/$^{13}CHCl_3$ and $CHCl_3$/$CDCl_3$ are shown in Figures 3 and 4. Kinetic isotope effects of $k_{CHCl_3+Cl}/k_{^{13}CHCl_3+Cl} = 1.000 \pm 0.003$ and $k_{CHCl_3+Cl}/k_{CDCl_3+Cl} = 3.283 \pm 0.011$ were derived from the slopes of the graphs.

3.1.2. OH Radical Reaction. The reactions of the chloroform isotopologues with hydroxyl radicals result in the stable products water, phosgene, and hypochlorous acid, HOCl. The initial reaction between chloroform and hydroxyl radical, reaction 12, is followed by reactions 9−11 to yield the phosgene product

$$CHCl_3 + OH \rightarrow CCl_3 + H_2O \quad (12)$$

The Cl resulting from reaction 11 will compete with OH to react with chloroform. However, H_2 is in large excess compared with chloroform, and the Cl atoms will be consumed by reaction with H_2, so this potential interference can be neglected. Because of the presence of both OH radicals and ozone, hydroperoxy radicals will be produced in the chamber

$$OH + O_3 \rightarrow HO_2 + O_2 \quad (13)$$

These hydroperoxy radicals will compete with the self reaction of $OOCCl_3$, resulting in CCl_3OOH or $OCCl_3$ according to reactions 14 and 15. The product of reaction 14 will decompose into phosgene and hypochlorous acid according to reaction 16.

$$OOCCl_3 + HO_2 \rightarrow CCl_3OOH + O_2 \quad (14)$$

$$OOCCl_3 + HO_2 \rightarrow OCCl_3 + O_2 + OH \quad (15)$$

$$CCl_3OOH \rightarrow COCl_2 + HOCl \quad (16)$$

Reactions 10 and 14 have similar rates (4.07×10^{-12} and 4.9×10^{-12} cm^3 molecule^{-1} s^{-1}),[35] and because of high concentrations of OH and ozone, concentrations of HO_2 are likely to be higher than concentrations of $OOCCl_3$, favoring reactions 14 and 15. Another possible reaction partner for $OOCCl_3$ is ozone, resulting in $OCCl_3$ production and thus phosgene. All of the mentioned reaction series will result in the production of Cl atoms, either through reaction 11 or as a result of photolysis of HOCl that is readily photolyzed at the wavelength of the lamp used in the experiment

$$HOCl + h\nu \rightarrow OH + Cl \quad (17)$$

Whereas up to one Cl may be produced by these processes for every OH that reacts with $CHCl_3$, the ratio $(k_{Cl+H_2}[H_2])/(k_{Cl+CHCl_3}[CHCl_3])$ is ca. 200, which means that less than 1% of the Cl that is produced will react with $CHCl_3$. The resulting correction to the KIE is insignificant.

The spectra from the reactions are demanding to analyze because of the presence of ozone at concentrations that produce saturated absorption bands. The strong $\nu_3(B_2)$ ozone band centered at about 1040 cm^{-1} could not be reproduced properly in the spectral analysis. Therefore the analysis was restricted to a narrower wavelength range than that of the analysis of the corresponding reactions with Cl. (See Table 1.) Figure 5 shows an example of a spectrum taken during the reaction of OH with $CHCl_3$ and $CDCl_3$. The $\nu_2(A_1)$ ozone band, centered around 700 cm^{-1}, is easily fitted in the analysis, as can be seen in the residual of the fit.

Relative rate plots of the decay of mixtures of $CHCl_3/^{13}CHCl_3$ and $CHCl_3/CDCl_3$ are shown in Figures 6 and 7. The kinetic isotope effects $k_{CHCl_3+OH}/k_{^{13}CHCl_3+OH} = 1.023 \pm 0.002$ and $k_{CHCl_3+OH}/k_{CDCl_3+OH} = 3.726 \pm 0.015$ were determined from the slopes of the graphs. That is, the kinetic isotope effect is larger

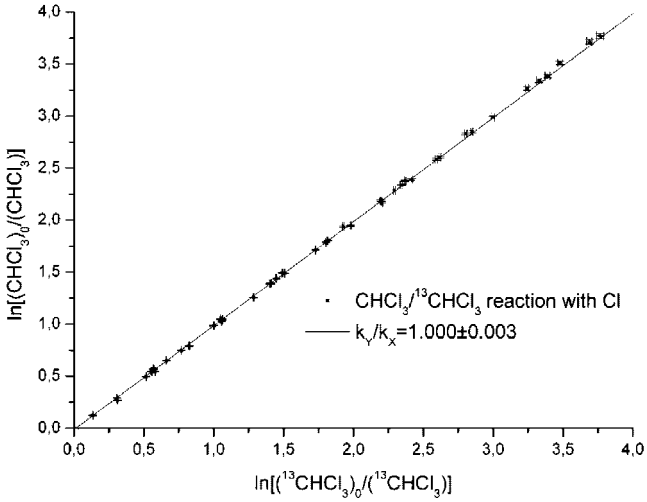

Figure 3. Relative rate plot showing the decay of $CHCl_3$ and $^{13}CHCl_3$ during reaction with Cl. 43 data points from 5 independent experiments give $k_{rel} = 1.000 \pm 0.003$.

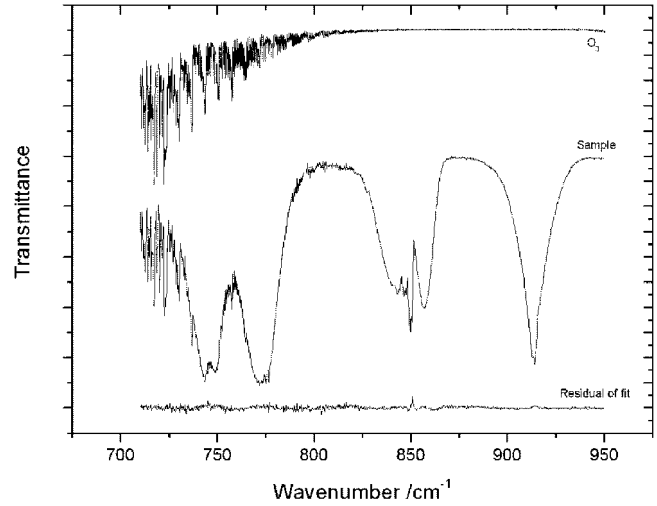

Figure 5. FTIR spectra of a $CHCl_3$ and $CDCl_3$ mixture during reaction with OH and residual of fit. Also included is the spectrum of ozone in the region.

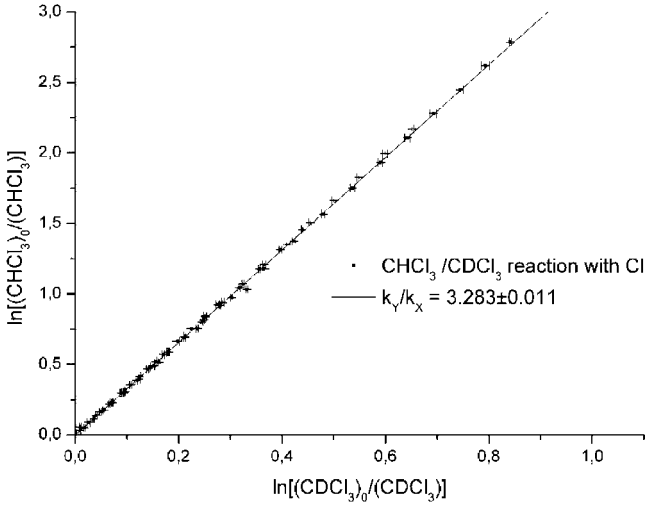

Figure 4. Relative rate plot showing the decay of $CHCl_3$ and $CDCl_3$ during reaction with Cl. 64 data points from 4 independent experiments give $k_{rel} = 3.283 \pm 0.011$.

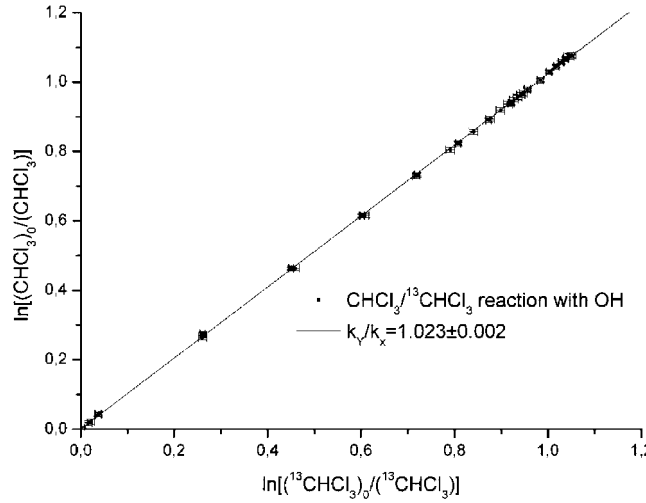

Figure 6. Relative rate plot showing the decay of $CHCl_3$ and $^{13}CHCl_3$ during reaction with OH. 50 data points from 3 independent experiments give $k_{rel} = 1.023 \pm 0.002$.

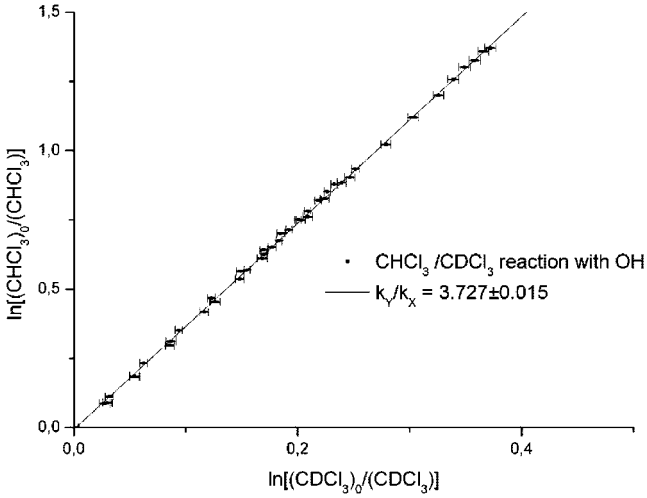

Figure 7. Relative rate plot showing the decay of $CHCl_3$ and $CDCl_3$ during reaction with OH. 42 data points from 4 independent experiments give $k_{rel} = 3.727 \pm 0.015$.

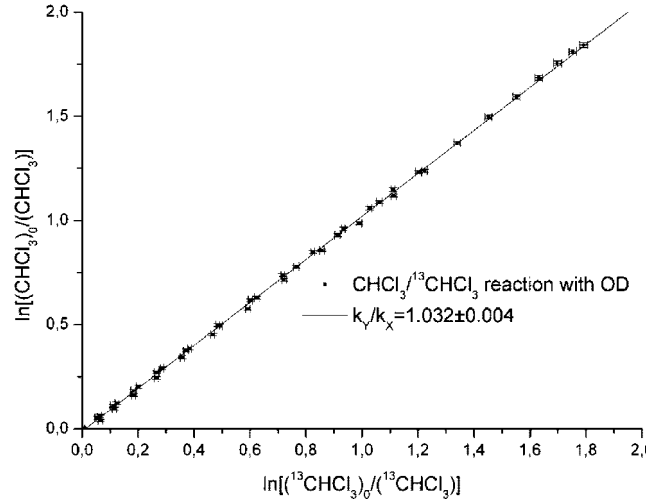

Figure 8. Relative rate plot showing the decay of $CHCl_3$ and $^{13}CHCl_3$ during reaction with OD. 43 data points from 3 independent experiments give $k_{rel} = 1.032 \pm 0.004$.

TABLE 2: Summary of Experimental Results and Comparison with Kinetic Isotope Effects in the Reactions of Chloromethane and Methane

	kinetic isotope effects		
isotopologues	Cl	OH	OD
$CHCl_3/CDCl_3$	3.28 ± 0.01	3.73 ± 0.02	3.95 ± 0.03
$CHCl_3/^{13}CHCl_3$	1.000 ± 0.003	1.023 ± 0.002	1.032 ± 0.004
CH_2Cl_2/CD_2Cl_2[39]	3.62 ± 0.04	4.05 ± 0.07	
$CH_2Cl_2/CHDCl_2$[39]	1.582 ± 0.024	1.84 ± 0.04	
$CH_2Cl_2/^{13}CH_2Cl_2$[39]	1.039 ± 0.005		
CH_3Cl/CD_3Cl[40]	4.91 ± 0.07	3.9 ± 0.4	
CH_3Cl/CHD_2Cl[41]	2.27 ± 0.04	2.03 ± 0.05	
CH_3Cl/CH_2DCl[41]	1.42 ± 0.04	1.41 ± 0.05	
$CH_3Cl/^{13}CH_3Cl$[40]	1.070 ± 0.010	1.059 ± 0.008	
CH_4/CD_4[42]	14.7 ± 0.3	7.36 ± 0.88	
CH_4/CHD_3[42]	4.73 ± 0.04	3.30 ± 0.50	
CH_4/CH_2D_2[42]	2.43 ± 0.02	1.81 ± 0.28	
CH_4/CH_3D[42]	1.459 ± 0.006	1.25 ± 0.14	
$CH_4/^{13}CH_4$[42]	1.06 ± 0.01	1.0039 ± 0.0004	
CH_3OH/CD_3OH[37]	3.011 ± 0.059	2.566 ± 0.042	
CH_3OH/CHD_2OH[37]	1.536 ± 0.060	1.326 ± 0.021	
CH_3OH/CH_2DOH[37]	1.162 ± 0.022	1.119 ± 0.045	
$CH_3OH/^{13}CH_3OH$[37]	1.055 ± 0.016	1.031 ± 0.020	

for the reactions of chloroform with OH than for the corresponding reactions with Cl. This is the same trend as that for the reaction of methylene chloride, CH_2Cl_2, with OH and Cl, whereas the opposite is true for methane, CH_4, and methyl chloride, CH_3Cl. (See Table 2.) This different ordering of the kinetic isotope effects is a motivation for further investigation of the system using computational methods.

3.1.3. OD Radical Reaction. The features of the spectra from the reaction between chloroform and OD radicals are much the same as those for the reactions with OH radicals. An additional complication in the analysis is the production of deuterated water (HDO, D_2O) and deuterated hypochlorous acid (DOCl).

Relative rate plots of the decay of mixtures of $CHCl_3/^{13}CHCl_3$ and $CHCl_3/CDCl_3$ are shown in Figures 8 and 9. From the slopes of the graphs, we find the kinetic isotope effects $k_{CHCl_3+OD}/k_{^{13}CHCl_3+OD} = 1.032 \pm 0.004$ and $k_{CHCl_3+OD}/k_{CDCl_3+OD} = 3.948 \pm 0.026$. That is, the isotope effect is larger in this reaction than for the corresponding reactions with the normal hydroxyl radical.

3.2. Computational Study. ***3.2.1. Electronic Structure and Frequency Calculations.*** There is an overestimation of the experimental values of bond lengths and angles by less than 1% in the optimized molecular structure of $CHCl_3$; this is consistent with previous studies at the same level of theory.[19,36]

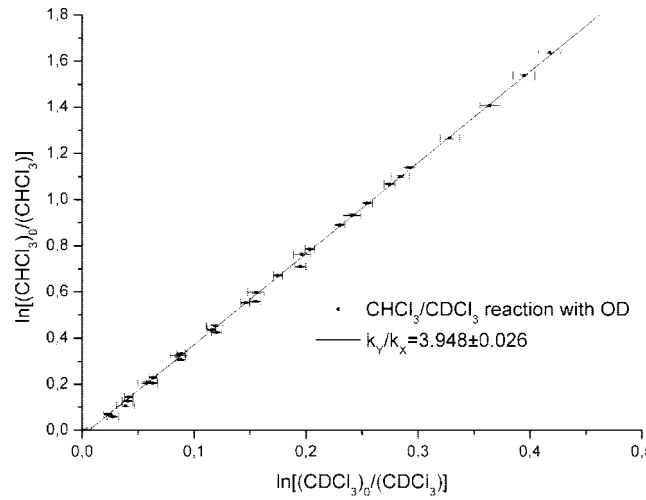

Figure 9. Relative rate plot showing the decay of $CHCl_3$ and $CDCl_3$ during reaction with OD. 34 data points from 3 independent experiments give $k_{rel} = 3.948 \pm 0.026$.

Structures of saddle points of the two reactions, optimized at the MP2/aug-cc-pVXZ (X = D, T) levels, are shown in Figure 10. The saddle point structure of the reaction with hydroxyl radical has C_s symmetry, whereas the corresponding structure for the chlorine reaction has C_{3v} symmetry. We note that the larger basis set gives slightly more reactant-like saddle points than the smaller basis set.

The rotational barrier for the OH group in the saddle point structure for the $CHCl_3$ + OH reaction was calculated to be 80.5 cm^{-1} at the MP2/aug-cc-PVDZ level of theory.

3.2.2. Reaction Path Following and Rate Constants. Figure 11 shows the minimum energy path, V_{MEP}, and the vibrational adiabatic potential energy curve, V^G_a, as a function of the reaction coordinate for the $CHCl_3$ + Cl reaction, and Figure S1 in the Supporting Information shows the vibrational frequencies calculated in POLYRATE using electronic structure data calculated at the CCSD(T)/aug-cc-PVTZ//MP2/aug-cc-PVDZ level of theory as a function of the reaction coordinate. The corresponding data for the reaction between chloroform and the hydroxyl radical are shown in Figure 12 and Figure S2 in the Supporting Information. The chlorine reaction has a medium

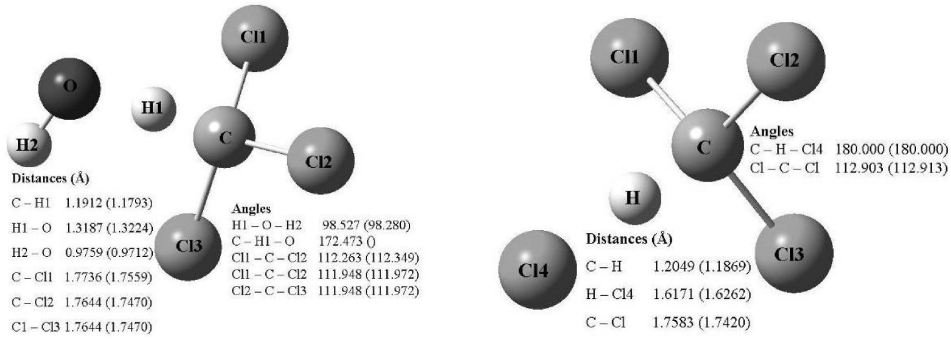

Figure 10. MP2/aug-cc-PVDZ and MP2/aug-cc-PVTZ (in parentheses) structures of the transition states $H-O-H-CCl_3$ and $Cl-H-CCl_3$.

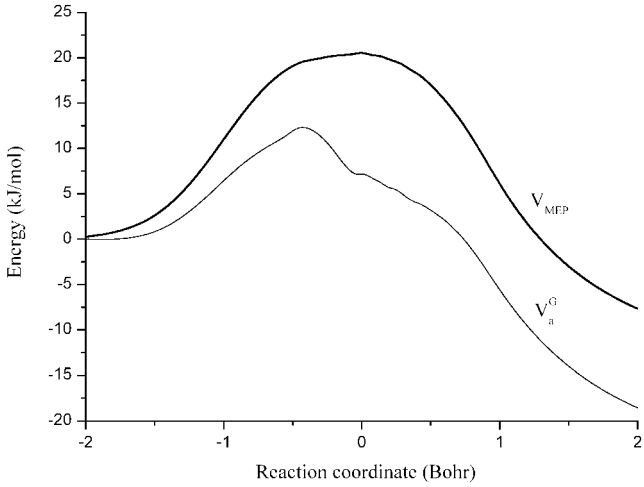

Figure 11. Minimum energy, V_{MEP}, and vibrational adiabatic potential energy curve, V^G_a, as a function of reaction coordinate for the $CHCl_3 + Cl \rightarrow CCl_3 + HCl$ reaction. Electronic structure data calculated at the CCSD(T)/aug-cc-PVTZ//MP2/aug-cc-PVDZ level of theory used as input for the reaction rate calculations.

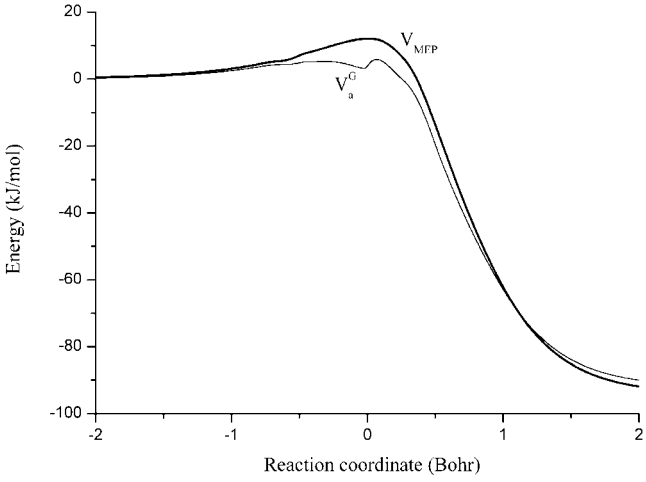

Figure 12. Minimum energy path, V_{MEP}, and vibrational adiabatic potential energy curve, V^G_a, as function of the reaction coordinate for the $CHCl_3 + OH \rightarrow CCl_3 + H_2O$ reaction. Electronic structure data calculated at the CCSD(T)/aug-cc-PVTZ//MP2/aug-cc-PVDZ level of theory used as input for the reaction rate calculations.

height (17.0 kJ/mol) and broad reaction barrier. The barrier for the hydroxyl radical reaction is somewhat lower (12.2 kJ/mol) but much narrower. Energetics of the reactions of chloroform, methylene chloride, methyl chloride, and methane with Cl and OH, calculated at the MP2/aug-cc-PVDZ//CCSD(T)/aug-cc-PVTZ level of theory, are presented in Table S3 in the Supporting Information. For both reactions, the C−H stretching

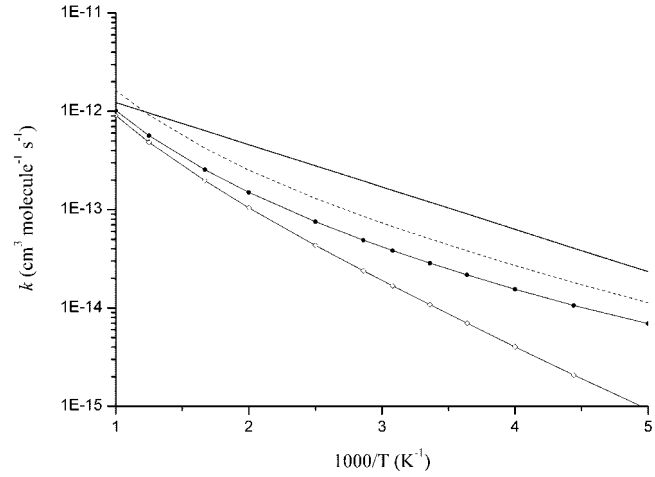

Figure 13. Arrhenius plot for the $CHCl_3 + Cl$ reaction. Thicker full drawn line: JPL recommendation; dashed line: TST; line with filled symbols: CVT/SCT with contribution from spin orbit coupling; line with open symbols: CVT/SCT. Electronic structure data calculated at the CCSD(T)/aug-cc-PVTZ//MP2/aug-cc-PVDZ level of theory used as input for the reaction rate calculations.

mode of chloroform is the reactive mode, as indicated by the dramatic decrease in the vibrational frequency in the vicinity of the saddle point. Figure 13 shows the calculated TST, CVT/

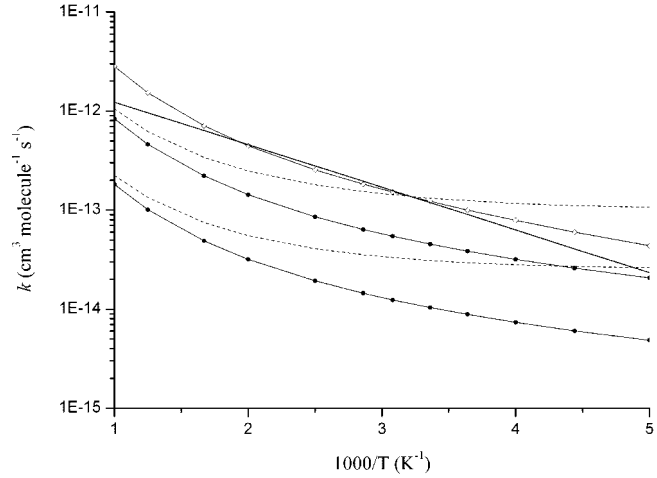

Figure 14. Arrhenius plot for the $CHCl_3 + OH$ reaction. Thick full drawn line: JPL recommendation, full drawn line with open symbols: TST; dashed lines: CVT/SCT, upper one with hindered rotor approximation; lines with filled symbols: CVT/SCT with contribution from spin orbit coupling, upper one with hindered rotor approximation. Electronic structure data calculated at the CCSD(T)/aug-cc-PVTZ//MP2/aug-cc-PVDZ level of theory used as input for the reaction rate calculations.

TABLE 3: Summary of Calculated and Experimental KIES at 298 K[a]

isotope reaction	KIE_{TST}	KIE_{CVT}	KIE_{CUS}	$KIE_{CVT/SCT}$	$KIE_{CUS/SCT}$	exptl results
$CDCl_3 + Cl$	7.94	3.10	3.24	3.85	4.03	3.28 ± 0.01
$^{13}CHCl_3 + Cl$	1.0088	1.0032	1.0034	1.0010	1.0012	1.000 ± 0.003
$CDCl_3 + OH$	7.14	7.48	7.48	4.05	4.05	3.73 ± 0.02
$^{13}CHCl_3 + OH$	1.0061	1.0105	1.0105	1.0096	1.0096	1.023 ± 0.002
$CDCl_3 + OD$	7.11	6.72	6.56	2.99	2.92	3.95 ± 0.03
$^{13}CHCl_3 + OD$	1.0057	1.0102	0.9864	0.9480	0.9256	1.032 ± 0.004

[a] $KIE = k_{CHCl_3+X}/k_{isotopereaction}$ where X = Cl, OH, OD.

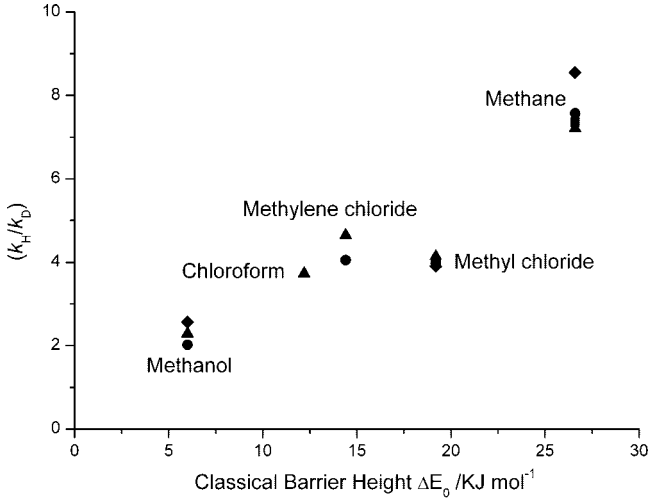

Figure 15. Classical barrier height versus per-atom H/D KIEs in the reaction with OH radicals for methane, methyl chloride, methylene chloride, chloroform, and methanol. ▲, D; ●, D_2; ◆, D_3; ■, D_4.

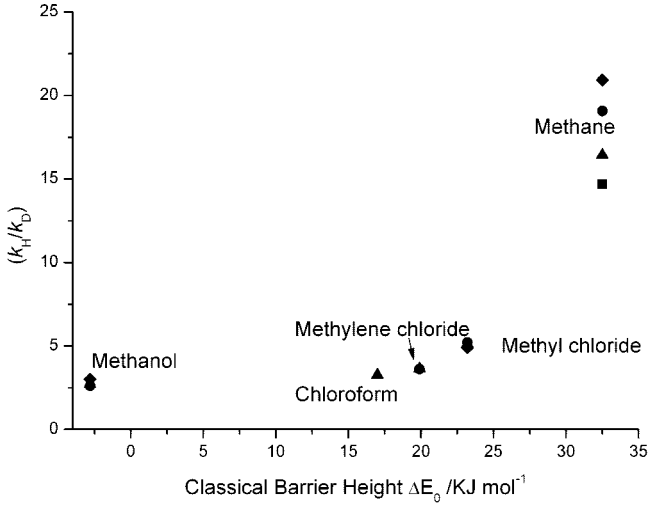

Figure 16. Classical barrier height versus normalized per-atom H/D KIEs in the reaction with Cl atoms for methane, methyl chloride, methylene chloride, chloroform and methanol. Spin orbit coupling is not included in the calculated barrier heights; contribution from spin orbit coupling would give methanol a small positive barrier.[37] ▲, D, ●; D_2, ◆; D_3, ■; D_4.

SCT, and CUS/SCT rate constants in the temperature range of 200−1000 K for the $CHCl_3 + Cl$ reaction, together with the values currently recommended by JPL.[16] The Arrhenius-type temperature dependence in the recommendation is not reproduced by the calculations; the deviation in the results increases as the temperature decreases and is taken to be an indication of complex formation in the reaction.

An Arrhenius plot for the $CHCl_3 + OH$ reaction is shown in Figure 14. This Figure includes the JPL experimentally derived rate recommendation, the TST rate constants, and the CVT rate constants with small curvature tunneling contribution. CVT/SCT results are presented for two different treatments of the C−H−OH torsional mode in the transition state, harmonic oscillator and hindered rotor. The hindered rotor treatment of the C−H−OH torsional mode is essential in this case and results in a decent reproduction of the experimental results.

3.2.3. Kinetic Isotope Effects. Table 3 summarizes the calculated and experimental kinetic isotope effects for the investigated reactions at 298 K. The table includes the values obtained from regular transition state theory, canonical variational transition state theory, and canonical unified statistical theory. CVT and CUS results are presented with and without small curvature tunneling.

3.2.3.1. Deuterium Isotope Effects. From the difference between TST and CVT results, one can see that the variational effect is pronounced in the reaction between chloroform and chlorine atoms and is less important in the reaction with hydroxyl radical isotopologues. For the chlorine reaction, the variational effect is larger in the parent molecule reaction than in the deuterated molecule reaction, lowering the KIE. The fact that the variational effect is important implies that translations along the imaginary degree of freedom at the transition state are linked to the vibrational degrees of freedom at relatively short distances along the reaction coordinate from the transition state. This is further supported by the rapid change in vibrational frequencies close to the transition state. (See Figure S1 in the Supporting Information.) The vibrational frequencies for the OH reaction do not change as dramatically; here only the reacting mode shows a large change. (See Figure S2 in the Supporting Information.)

From Table 3, it is clear that the tunneling effect should be included to give reasonable results for the kinetic isotope effects. It is interesting to note that for the reactions with chlorine atoms, the inclusion of the tunneling contribution increases the kinetic isotope effect, whereas the opposite is true for the reaction with the hydroxyl radical. Because tunneling occurs more easily for the lighter species (H) compared with heavier (D) species, tunneling effects are normally expected to favor the reaction of the lighter isotopologues, giving a larger isotope effect, as in the case of the reaction $CHCl_3 + Cl$. The opposite trend can be seen when the reaction barrier is sufficiently low; in these cases, the change in zero-point energy (ZPE) resulting from deuteration makes a relatively large contribution to the barrier. This larger barrier results in a larger tunneling probability for the deuterated species. The same effect is seen in calculations on the $CH_3OH + OH$[37] and $CH_3F + OH$[38] reactions.

The reaction between chloroform and deuterated hydroxyl radicals, OD, has the largest isotope effect in the experimental part of this study. The trend is not reproduced in the calculations, where the isotope effect is underestimated.

3.2.3.2. ^{13}C Isotope Effects. For the reactions involving carbon 13, the calculated CVT/SCT and CUS/SCT results are in the same order as the experimental results: $KIE_{CHCl_3+OH} > KIE_{CHCl_3+Cl}$. The calculated results overestimate the experimental results for the chlorine reaction and underestimate the results for the hydroxyl radical reactions. The opposite is seen for the isotope effects in the reaction between chloroform and OD; experimentally, this is the largest of the ^{13}C isotope effects, whereas the calculations predict an inverse isotope effect.

3.2.3.3. Temperature Dependence in the Isotope Effect. Table S1 in the Supporting Information shows the kinetic isotope effects for the reaction between chlorine and chloroform isotopologues in the temperature range of 200−1000 K. The temperature dependence of the KIE is strong for the reaction with the deuterated species, and the tunneling contribution becomes less important as the temperature increases. The temperature dependence and the role of tunneling are small in the reaction with the ^{13}C species. The trends are similar for the reactions with hydroxyl radicals (Table S2 in the Supporting Information), except that the tunneling contribution is more important for the $^{13}CHCl_3 + OD$ reaction than for the other reactions with ^{13}C species.

4. Comparison and Discussion

In this work, we have presented experimental and theoretical kinetic isotope effects for the reactions between chloroform isotopologues and the atmospherically relevant radicals OH and Cl. The study completes the investigations of OH and Cl reactivity with the series of compounds $CH_{4-n}Cl_n$ for $n = 0$ to 4. A summary of experimental kinetic isotope effects from this study and recent studies of reactions of CH_4, CH_3Cl, CH_2Cl_2, and CH_3OH with OH and Cl is shown in Table 2. Increasing number of chlorines decreases the kinetic isotope effect in the fully deuterated species. A trend for methane and methyl chloride is that the isotope effects are larger for the reactions with chlorine than for the reactions with hydroxyl radicals. For chloroform and methylene chloride, the trend is the opposite with larger isotope effects for the OH reactions. The reaction barriers are generally higher for the reactions with Cl atoms than for reactions with OH. The table also shows that the reaction barrier is lowered with an increased number of chlorines.

We have evaluated the deuterium isotope effects in the reactions of the chloromethanes, methanol, and methane with OH and Cl. The common standard is the relative reactivity of a hydrogen/deuterium atom in each molecule. We assume that the reaction rate for each molecule is the linear sum of per-atom reaction rates. For example, the KIE k_{CH_3Cl}/k_{CHD_2Cl} is due to $3k_H/(k_H + 2k_D)$. When this KIE is multiplied by $(KIE(k_H/k_D) + 2)/3$, the ratio k_H/k_D for $CHD_2Cl + Cl$ results, termed the "algebraic k_H/k_D ratio". $KIE(k_H/k_D)$ is determined using k_{CH_3Cl}/k_{CD_3Cl}. The algebraic k_H/k_D ratio is seen to vary with the classical reaction barrier for both the Cl and OH reactions, as shown in Figures 15 and 16. The reaction barrier increases with decreasing chlorination; from left to right, the Figures show methanol, chloroform, methylene chloride, methyl chloride, and methane. The k_H/k_D ratio increases with the barrier height, clearly showing the increased reactivity of H relative to D. The cause of the kinetic isotope effects for these reactions can be divided into two essential parts; tunneling and change in ZPE. As the barrier height increases, the role of tunneling increases, favoring the reaction of the lighter species. For the reactions with lower barrier heights, the change in ZPE is more important for the kinetic isotope effects. One result of this is the scatter we see in the points for each compound in Figure 15. In the OH reactions, the change in ZPE is important, and because every added deuterium increases the ZPE, the relative reactivity of H changes with the number of deuterium substitutions.

Acknowledgment. This work is part of the ACTION (Atmospheric Chemistry and Transport from Isotopic Analysis) project supported by the Norwegian Research Council. M.S.J. and E.J.K.N. thank the Copenhagen Center for Atmospheric Research supported by the Danish Natural Science Research Council and the Villum Kahn Rasmussen Fund. We thank A. A. Gola and coworkers for making their results on the OH and Cl reactions with CH_2Cl_2 available prior to publication. E.J.K.N. thanks J. Heimdal for useful comments on the theoretical calculations.

Supporting Information Available: Kinetic isotope effects for the reactions $CHCl_3 + Cl \rightarrow CCl_3 + HCl$ and $CHCl_3 + OH \rightarrow CCl_3 + H_2O$ in the temperature range 200−1000 K. Energetics of reactions of chlorinated methane derivatives with Cl and OH. Plots of vibrational frequencies in the $CHCl_3 + Cl \rightarrow CCl_3 + HCl$ and $CHCl_3 + OH \rightarrow CCl_3 + H_2O$ reactions are provided. This material is available free of charge via the Internet at http://pubs.acs.org.

References and Notes

(1) Khalil, M. A. K.; Rasmussen, R. A. *Atmos. Environ.* **1999**, *33*, 1151.
(2) McCulloch, A. *Chemosphere* **2003**, *50*, 1291.
(3) Worton, D. R.; Sturges, W. T.; Schwander, J.; Mulvaney, R.; Barnola, J. M.; Chappellaz, J. *Atmos. Chem. Phys.* **2006**, *6*, 2847.
(4) Aucott, M. L.; McCulloch, A.; Graedel, T. E.; Kleiman, G.; Midgley, P.; Li, Y. F. *J. Geophys. Res., [Atmos.]* **1999**, *104*, 8405.
(5) Trudinger, C. M.; Etheridge, D. M.; Sturrock, G. A.; Fraser, P. J.; Krummel, P. B.; McCulloch, A. *J. Geophys. Res., [Atmos.]* **2004**, *109*, D22310.
(6) Laturnus, F.; Haselmann, K. F.; Borch, T.; Gron, C. *Biogeochemistry* **2002**, *60*, 121.
(7) Khalil, M. A. K.; Moore, R. M.; Harper, D. B.; Lobert, J. M.; Erickson, D. J.; Koropalov, V.; Sturges, W. T.; Keene, W. C. *J. Geophys. Res., [Atmos.]* **1999**, *104*, 8333.
(8) Brahan, K. M.; Hewitt, A. D.; Boone, G. D.; Hewitt, S. A. *Int. J. Chem. Kinet.* **1996**, *28*, 397.
(9) Beichert, P.; Wingen, L.; Lee, J.; Vogt, R.; Ezell, M. J.; Ragains, M.; Neavyn, R.; Finlayson-Pitts, B. J. *J. Phys. Chem.* **1995**, *99*, 13156.
(10) Orlando, J. J. *Int. J. Chem. Kinet.* **1999**, *31*, 515.
(11) Bryukov, M. G.; Slagle, I. R.; Knyazev, V. D. *J. Phys. Chem. A* **2002**, *106*, 10532.
(12) Howard, C. J.; Evenson, K. M. *J. Chem. Phys.* **1976**, *64*, 4303.
(13) Davis, D. D.; Machado, G.; Conaway, B.; Oh, Y.; Watson, R. *J. Chem. Phys.* **1976**, *65*, 1268.
(14) Taylor, P. H.; Jiang, Z.; Dellinger, B. *Int. J. Chem. Kinet.* **1993**, *25*, 9.
(15) Hsu, K. J.; DeMore, W. B. *Geophys. Res. Lett.* **1994**, *21*, 805.
(16) Sander, S. P.; Friedl, R. R.; Ravishankara, A. R.; Golden, D. M.; Kolb, C. E.; Kurylo, M. J.; Molina, M. J.; Moortgat, G. K.; Keller-Rudek, H.; Finlayson-Pitts, B. J.; Wine, P. H.; Huie, R. E.; Orkin, V. L. *Chemical Kinetics and Photochemical Data for Use in Atmospheric Studies, Evaluation Number 15*; JPL Publication 06-2; National Aeronautics and Space Administration, Jet Propulsion Laboratory, California Institute of Technology: Pasadena, CA, 2006.
(17) Kryachko, E. S.; Zeegers-Huyskens, T. *J. Mol. Struct.* **2002**, *615*, 251.
(18) Kryachko, E. S.; Zeegers-Huyskens, T. *J. Phys. Chem. A* **2002**, *106*, 6832.
(19) Jalili, S.; Akhavan, M. *J. Mol. Struct.: THEOCHEM* **2006**, *765*, 105.
(20) Johnson, M. S.; Feilberg, K. L.; von Hessberg, P.; Nielsen, O. J. *Chem. Soc. Rev.* **2002**, *31*, 313.
(21) Aker, P. M.; Sloan, J. J. *J. Chem. Phys.* **1986**, *85*, 1412.
(22) Huang, Y.; Gu, Y.; Liu, C.; Yang, X.; Tao, Y. *Chem. Phys. Lett.* **1986**, *127*, 432.
(23) Streit, G. E.; Whitten, G. Z.; Johnston S., H. *Geophys. Res. Lett.* **1976**, *3*, 521.

(24) D'Ottone, L.; Bauer, D.; Campuzano-Jost, P.; Fardy, M.; Hynes, A. J. *Phys. Chem. Chem. Phys.* **2004**, *6*, 4276.
(25) Griffith, D. W. T. *Appl. Spectrosc.* **1996**, *50*, 59.
(26) Rothman, L. S.; Jacquemart, D.; Barbe, A.; Benner, D. C.; Birk, M.; Brown, L. R.; Carleer, M. R.; Chackerian, C.; Chance, K.; Coudert, L. H.; Dana, V.; Devi, V. M.; Flaud, J. M.; Gamache, R. R.; Goldman, A.; Hartmann, J. M.; Jucks, K. W.; Maki, A. G.; Mandin, J. Y.; Massie, S. T.; Orphal, J.; Perrin, A.; Rinsland, C. P.; Smith, M. A. H.; Tennyson, J.; Tolchenov, R. N.; Toth, R. A.; Vander Auwera, J.; Varanasi, P.; Wagner, G. *J. Quant. Spectrosc. Radiat. Transfer* **2005**, *96*, 139.
(27) Frisch, M. J.; Trucks, G. W.; Schlegel, H. B.; Scuseria, G. E.; Robb, M. A.; Cheeseman, J. R.; Montgomery, J. A., Jr.; Vreven, T.; Kudin, K. N.; Burant, J. C.; Millam, J. M.; Iyengar, S. S.; Tomasi, J.; Barone, V.; Mennucci, B.; Cossi, M.; Scalmani, G.; Rega, N.; Petersson, G. A.; Nakatsuji, H.; Hada, M.; Ehara, M.; Toyota, K.; Fukuda, R.; Hasegawa, J.; Ishida, M.; Nakajima, T.; Honda, Y.; Kitao, O.; Nakai, H.; Klene, M.; Li, X.; Knox, J. E.; Hratchian, H. P.; Cross, J. B.; Bakken, V.; Adamo, C.; Jaramillo, J.; Gomperts, R.; Stratmann, R. E.; Yazyev, O.; Austin, A. J.; Cammi, R.; Pomelli, C.; Ochterski, J. W.; Ayala, P. Y.; Morokuma, K.; Voth, G. A.; Salvador, P.; Dannenberg, J. J.; Zakrzewski, V. G.; Dapprich, S.; Daniels, A. D.; Strain, M. C.; Farkas, O.; Malick, D. K.; Rabuck, A. D.; Raghavachari, K.; Foresman, J. B.; Ortiz, J. V.; Cui, Q.; Baboul, A. G.; Clifford, S.; Cioslowski, J.; Stefanov, B. B.; Liu, G.; Liashenko, A.; Piskorz, P.; Komaromi, I.; Martin, R. L.; Fox, D. J.; Keith, T.; Al-Laham, M. A.; Peng, C. Y.; Nanayakkara, A.; Challacombe, M.; Gill, P. M. W.; Johnson, B.; Chen, W.; Wong, M. W.; Gonzalez, C.; Pople, J. A. *Gaussian 03*, revision C.02; Gaussian, Inc.: Wallingford, CT, 2004.
(28) Gonzalez, C.; Schlegel, H. B. *J. Phys. Chem.* **1990**, *94*, 5523.
(29) Corchado, J. C.; Coitino, E. L.; Chuang, Y. Y.; Fast, P. L.; Truhlar, D. G. *J. Phys. Chem. A* **1998**, *102*, 2424.
(30) Corchado, J. C.; Chuang, Y. Y.; Fast, P. L.; Villà, J.; Hu, W.-P.; Liu, Y.-P.; Lynch, G. C.; Nguyen, K. A.; Jackels, C. F.; Melissas, V. S.; Lynch, B. J.; Rossi, I.; Coitiño, E. L.; Fernandez-Ramos, A.; Pu, J.; Albu, T. V.; Steckler, R.; Garrett, B. C.; Isaacson, A. D.; Truhar, D. G. *POLYRATE*; University of Minnesota: Minneapolis, 2002.
(31) Fast, P. L.; Corchado, J. C.; Truhlar, D. G. *J. Chem. Phys.* **1998**, *109*, 6237.
(32) Garrett, B. C.; Truhlar, D. G. *J. Phys. Chem.* **1979**, *83*, 1052.
(33) Chuang, Y. Y.; Corchado, J. C.; Truhlar, D. G. *J. Phys. Chem. A* **1999**, *103*, 1140.
(34) Chuang, Y. Y.; Truhlar, D. G. *J. Chem. Phys.* **2000**, *112*, 1221.
(35) Catoire, V.; Lesclaux, R.; Schneider, W. F.; Wallington, T. J. *J. Phys. Chem.* **1996**, *100*, 14356.
(36) Colmont, J. M.; Priem, D.; Drean, P.; Demaison, J.; Boggs, J. E. *J. Mol. Spectrosc.* **1998**, *191*, 158.
(37) Feilberg, K. L.; Gruber-Stadler, M.; Johnson, M. S.; Muhlhauser, M.; Nielsen, C. J. *J. Phys. Chem. A* **2008**, *112*, 11099.
(38) Marinkovic, M.; Gruber-Stadler, M.; Nicovich, J. M.; Soller, R.; Muhlhauser, M.; Wine, P. H.; Bache-Andreassen, L. *J. Phys. Chem. A* **2008**, *112*, 12416.
(39) Gola, A. A.; Bache-Andreassen, L.; Sellevag, S. R.; Nielsen, C. J., unpublished results.
(40) Gola, A. A.; D'Anna, B.; Feilberg, K. L.; Sellevag, S. R.; Bache-Andreassen, L.; Nielsen, C. J. *Atmos. Chem. Phys.* **2005**, *5*, 2395.
(41) Sellevag, S. R.; Nyman, G.; Nielsen, C. J. *J. Phys. Chem. A* **2006**, *110*, 141.
(42) Feilberg, K. L.; Griffith, D. W. T.; Johnson, M. S.; Nielsen, C. J. *Int. J. Chem. Kinet.* **2005**, *37*, 110.

JP807233X